ACS Photonics

pubs.acs.org/journal/apchd5

Letter

Fano Lineshapes and Rabi Splittings: Can They Be Artificially Generated or Obscured by the Numerical Aperture?

Zhoumuyan Geng, Johanna Theenhaus, Biplab K. Patra, Jian-Yao Zheng, Joris Busink, Erik C. Garnett, and Said R. K. Rodriguez*

Cite This: *ACS Photonics* 2021, 8, 1271−1276

Read Online

ACCESS | Metrics & More | Article Recommendations | Supporting Information

ABSTRACT: Fano resonances and Rabi splittings are routinely reported in the scientific literature. Asymmetric resonance lineshapes are usually associated with Fano resonances, and two split peaks in the spectrum are often attributed to a Rabi splitting. True Fano resonances and Rabi splittings are unequivocal signatures of coherent coupling between subsystems. However, can the same spectral lineshapes characterizing Fano resonances and Rabi splittings arise from a purely incoherent sum of intensities? Here we answer this question through experiments with a tunable Fabry-Pérot cavity containing a $CsPbBr_3$ perovskite crystal. By measuring the transmission and photoluminescence of this system using microscope objectives with different numerical aperture (NA), we find that even a modest $NA = 0.4$ can artificially generate Fano resonances and Rabi splittings. We furthermore show that this modest NA can obscure the anticrossing of a bona fide strongly coupled light−matter system. Through transfer matrix calculations we confirm that these spectral artifacts are due to the incoherent sum of transmitted intensities at different angles captured by the NA. Our results are relevant to the wide nanophotonics community, characterizing dispersive optical systems with high numerical aperture microscope objectives. We conclude with general guidelines to avoid pitfalls in the characterization of such optical systems.

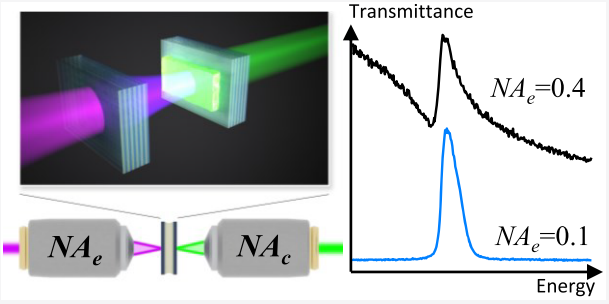

KEYWORDS: *Fano resonance, polariton, strong coupling, coupled oscillators, optical cavity, perovskite*

Fano resonances and Rabi splittings have inspired countless efforts in photonics research.[1−4] These two effects were discovered in quantum frameworks, yet their essence can be easily recognized in classical models of coupled harmonic oscillators.[5−7] When the oscillators are detuned and one is much more damped than the other, interference effects lead to an asymmetric Fano-like resonance in the spectrum of the heavily damped oscillator.[6] Conversely, when the two oscillators are strongly coupled, weakly damped, and tuned in resonance, the total energy is split between two new eigenmodes at different frequencies.[5,7] This is the so-called Rabi splitting or normal mode splitting. Within the classical framework, the main difference between the two effects sits in the ratio of the frequency detuning to the total loss rates of the oscillators. This ratio is large for a Fano resonance and close to zero for a Rabi splitting. The common aspect is the need for coherent coupling between two oscillators. Without this key ingredient, the bare oscillators simply display Lorentzian lineshapes around their resonance frequencies.

Interest in Fano resonances and Rabi splittings is so large that a complete list of references in photonics only is beyond our reach. Nonetheless, we can highlight a few scenarios where Fano resonances are relevant: sensing,[8,9] switching,[10] directional scattering,[2,11,12] spontaneous emission,[13] lasing,[14] and nonreciprocity.[15] Meanwhile, Rabi splittings have attracted interest for enhancing or modifying chemical landscapes,[16,17] optical nonlinearities,[18] electrical conductivities,[19,20] biological processes,[21] lasing,[22,23] and quantum light emission.[24,25] Key to progress in all these directions is the correct identification of Fano resonances and Rabi splittings based on optical measurements. A first challenge in this endeavor arises because the transmittance (T), reflectance (R), absorbance (A), and photoluminescence (PL), of a fixed light−matter system generally display different features.[26] In particular, Rabi splittings observed in T, R, A, and PL are, in general, all different. The differences can be so large that some observables display a well-resolved Rabi splitting, while other observables display no splitting at all. This effect has been discussed in the literature,[27,28] and coupled oscillator analogs can shed some light into its origin.[29] In this manuscript, we consider a second challenge in the identification of Fano resonances and Rabi

Received: January 23, 2021
Published: May 4, 2021

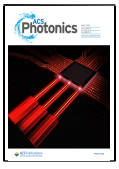

splittings, one that appears to have never been considered, yet is highly relevant to experiments. In particular, we ask the following: Can the numerical aperture(s) of the measuring instrument artificially generate or obscure Fano resonances and Rabi splittings? To address this question, we performed experiments with the simplest and most widely used optical resonator: a Fabry-Pérot cavity. Our cavity contains a perovskite crystal of contemporary interest, namely, $CsPbBr_3$.[30,31] Our coupled oscillator system is therefore one that comprises cavity photons and semiconductor excitons. As we will show, the choice of numerical aperture(s) used to probe this system conveys a number of surprises and spectral artifacts that can lead to misleading conclusions when not properly considered.

Figure 1a illustrates our experimental system: a tunable Fabry-Pérot cavity with a $CsPbBr_3$ crystal inside. $CsPbBr_3$ crystals were synthesized on a mica substrate via chemical vapor deposition (CVD).[32] Using thermal release tape, the crystals were subsequently transferred onto a glass substrate for characterization or onto a mirror for experiments. Figure 1b shows a dark-field image of a typical $CsPbBr_3$ crystal on a glass substrate. Figure 1c shows the absorbance and *PL* spectrum of the $CsPbBr_3$ crystal used in all our experiments discussed below. The absorbance spectrum has an excitonic peak at 2.397 ± 0.002 eV with a 66 meV line width, estimated via the Gaussian fit shown in Figure 1c. The *PL* spectrum is fitted with a Lorentzian line shape centered at 2.358 ± 0.002 eV and with 44 meV line width. We placed this crystal in our cavity, which is made by two distributed Bragg reflectors (DBRs) with a peak reflectance of 99.9% at 530 nm. The position and orientation of one of the cavity mirrors are controlled with a six degree-of-freedom piezoelectric actuator. The other mirror, coated with the $CsPbBr_3$ crystal, is mounted on three piezoelectric actuators. Two of the actuators are used to place the $CsPbBr_3$ crystal along the optical axis; the other actuator serves to finely adjust the cavity length. Using this setup, we measured the *T* and *PL* spectrum as a function of the cavity length. We use an incoherent white light source for *T* measurements and a 405 nm laser for *PL* measurements. Optical excitation and collection were achieved through microscope objectives with numerical aperture as specified for each figure below. We refer to the excitation *NA* as NA_e and to the collection *NA* as NA_c. For *T* measurements, we varied NA_e while keeping NA_c = 0.4 constant. For *PL* measurements, we varied NA_c while keeping NA_e = 0.25 constant. In the *PL* case, the choice NA_e = 0.25 is not so relevant because the incident laser is filtered out and we only collect the luminescence. Moreover, the laser power for all *PL* measurements is sufficiently low (40 μW at the excitation objective) to avoid nonlinear effects and crystal degradation.

Figure 2a shows *T* spectra of the $CsPbBr_3$-cavity system at a cavity length *L* = 3440 nm for three different NA_e. For NA_e = 0.1, we observe a nearly symmetric resonance peak on a flat background. The same optical resonance acquires a high-energy tail when NA_e increases to 0.25. Then, an asymmetric line shape resembling a Fano resonance appears for NA_e = 0.4. This line shape is not the result of Fano interference. Instead, it is an artifact of the large NA_e. As demonstrated ahead, the asymmetric line shape is due to the incoherent sum of transmitted intensities at different angles.

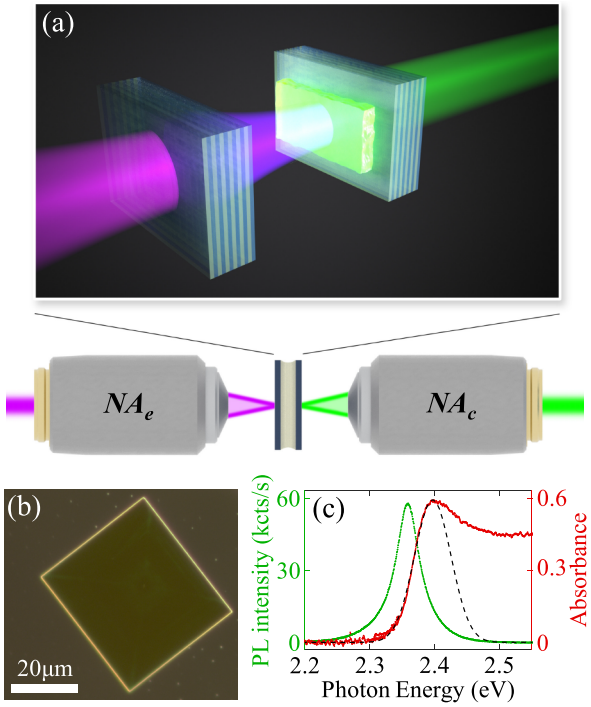

Figure 1. (a) Tunable cavity with a $CsPbBr_3$ crystal inside. The excitation light is coupled into the cavity through a microscope objective with numerical aperture NA_e and light is collected through a different objective with numerical aperture NA_c. (b) Dark-field microscope image of a typical $CsPbBr_3$ crystal on a glass substrate. (c) Absorbance and photoluminescence spectra of the $CsPbBr_3$ crystal used for the experiments in Figures 2, 3, and 5. The excitonic peak in the absorbance spectrum is fitted with a Gaussian distribution centered at 2.397 ± 0.002 eV and a standard deviation of 66 meV. The photoluminescence is fitted with a Lorentzian line shape centered at 2.358 ± 0.002 eV and with a 44 meV line width.

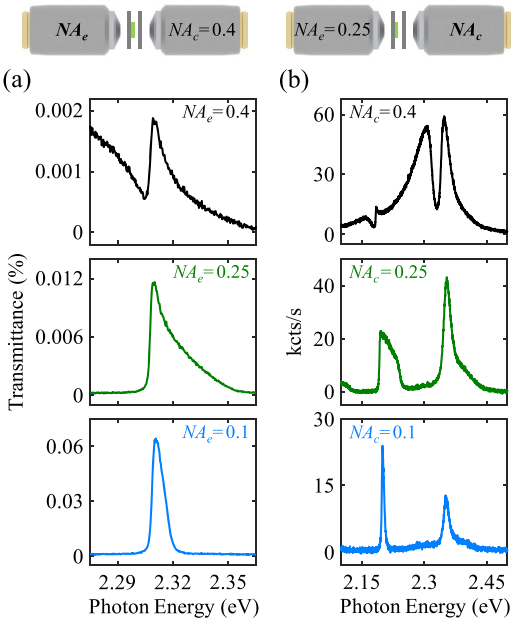

Figure 2. (a) Transmittance and (b) photoluminescence spectra of the $CsPbBr_3$-cavity system. In (a) we vary the excitation numerical aperture NA_e while keeping the collection numerical aperture NA_c = 0.4 constant. In (b) we vary NA_c while keeping NA_e = 0.25 constant. The cavity length is *L* = 3440 nm in (a) and *L* = 3360 nm in (b).

https://doi.org/10.1021/acsphotonics.1c00128
ACS Photonics 2021, 8, 1271−1276

Figure 2b shows *PL* spectra of the same $CsPbBr_3$-cavity system for a slightly different cavity length L = 3360 nm. For NA_c = 0.1, we observe two nearly symmetric resonance peaks on a flat background. Each of these peaks corresponds to a cavity resonance. For NA_c = 0.25, the peaks acquire a high-energy tail. For NA_c = 0.4, the measured spectrum displays two remarkable features: a feature resembling a Rabi splitting appears around 2.32 eV, and a Fano-like resonance appears around 2.18 eV. These spectral features, which only appear for a sufficiently large NA_c, are artifacts. They are due to the incoherent sum of the cavity-enhanced perovskite emission at different angles. The apparent Rabi splitting in Figure 2b, around 2.33 eV, is suspiciously close to the bare exciton energy at 2.397 eV. However, this proximity is only a coincidence. In order to elucidate the origin of all these artifacts, we proceed to inspect spectra across a wide range of cavity lengths.

Figure 3 shows *T* and *PL* spectra as a function of cavity length for the same configurations considered in Figure 2. For

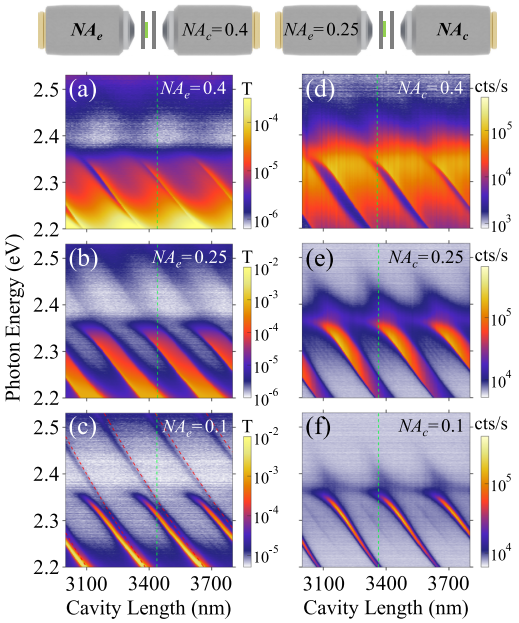

Figure 3. (a–c) Transmittance and (d–f) photoluminescence spectra of the $CsPbBr_3$-cavity system as a function of the cavity length. In (a)–(c) we vary the excitation numerical aperture NA_e while keeping the collection numerical aperture NA_c = 0.4 constant. In (d)–(f) we vary NA_c while keeping NA_e = 0.25 constant. The bright bands in all measurements correspond to resonances associated with different longitudinal mode numbers. The resonances are blurred at high energies by the bandgap absorption of $CsPbBr_3$. For reference, (c) shows empty cavity modes as red dashed lines. Green dashed lines in (a)–(c) and (d)–(f) indicate the cavity lengths inspected in Figure 2a and b, respectively.

reference, the vertical green dashed lines in Figure 3a–c (respectively, Figures 3d–f) indicate the cavity length considered in Figure 2a (respectively, Figure 2b). Each bright band in the color plot corresponds to a resonance associated with a particular longitudinal mode of the cavity. The longitudinal modes of the empty cavity are shown as red dashed lines in Figure 3c. Their resonance frequency satisfies $f = qc/2L$, with q the longitudinal mode number, c the speed of light, and L the cavity length.

We first analyze the *T* spectra in Figure 3a–c. Notice how as NA_e increases, all resonances broaden in energy. For NA_e = 0.4, shown in Figure 3a, the transmission from consecutive longitudinal modes nearly overlap. Only a narrow transmission dip between resonances remains. This is the Fano-like dip observed in Figure 2a. The results in Figure 3a–c already reveal the origin of the transmission dip: as NA_e increases, transmission bands associated with consecutive q increasingly approach each other in energy and eventually overlap. As Figure 3d–f show, similar behavior arises in the *PL* measurements when NA_c increases. For NA_c = 0.4, shown in Figure 3d, the emission from consecutive longitudinal modes nearly overlap in energy. The emission dip between bands with consecutive q, at fixed cavity length, results in features that can resemble Fano resonances or Rabi splittings but are neither.

Our measurements clearly demonstrate that even a moderately large *NA* can generate spectral features reminiscent of coherently coupled systems. Two important questions remain. First, are these spectral features due to the presence of an excitonic material in our cavity? Second, are interference effects responsible for these spectral features in any way? In the following, we will demonstrate that the answer to both of these questions is negative. We will analyze *T* spectra for an empty Fabry-Pérot cavity in experiments and theory. While this analysis is necessarily restricted to *T* (there is no *PL* in an empty cavity), the insights obtained from it are general.

Figure 4a shows experimental *T* spectra for the same three NA_e considered in Figures 2 and 3 and at a cavity length L =

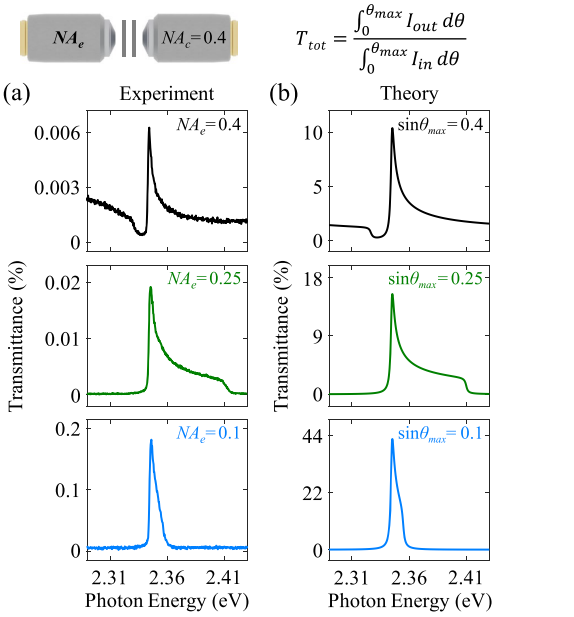

Figure 4. (a) Experimental transmittance spectra of an empty cavity for three different NA_e. (b) Transfer matrix calculations of transmittance spectra averaged over an angular range corresponding to the experimental NA_e. The averaged transmittance is given by the incoherent sum of transmitted intensities at different angles, divided by the incident intensity over the same angular range. The cavity length is L = 3430 nm in both experiments and calculations.

3430 nm. As NA_e increases, we again observe a broadening of the resonance and the emergence of a Fano-like line shape. This demonstrates how increasing NA_e generates a Fano-like line shape, even in the absence of an excitonic material. To identify the mechanism underlying this effect, we use a transfer matrix model to calculate the transmission of an empty cavity. Our goal is to determine whether the incoherent sum of

https://doi.org/10.1021/acsphotonics.1c00128
ACS Photonics 2021, 8, 1271–1276

transmitted intensities over a finite angular range can lead to Fano-like lineshapes.

Our transfer matrix calculations are done for a DBR−vacuum−DBR cavity. We model each DBR as a stack of six pairs of layers with refractive index n_1 = 1.45 and n_1 = 2.3. These values correspond, within the frequency range of interest, to our experimental DBRs made of silica and Ta_2O_5. We calculate the transmittance (i.e., transmitted power normalized to the incident power) when the cavity is illuminated by a single plane wave, and we vary the angle of incidence in steps of 0.005°. Then, we average the transmittance over the angular range corresponding to the NA_e of interest. We also sum the contributions of the two orthogonal polarizations, in correspondence to our experiments that were done using unpolarized light.

Figure 4b shows transfer matrix calculation results obtained, as described above, for the same cavity length considered in Figure 4a. Notice how the experimentally observed Fano-like lineshapes are reproduced in the calculations. This demonstrates that the sum of transmitted intensities at different incident angles suffices to generate Fano-like lineshapes. Since we are adding intensities and not field amplitudes, we are neglecting interference effects due to different plane waves. Hence, by reproducing the experimentally observed lineshapes in this way, we can conclude that the measured lineshapes are not due to Fano interference. We therefore call these Fano-like lineshapes "artifacts". While our calculations qualitatively reproduce the experimental lineshapes very well, the value of T is much lower in experiments. We attribute this difference to an imperfect alignment of the cavity mirrors, which leads to very significant optical losses through the sides of the cavity. Scattering losses may also reduce the value of T in experiments, but we suspect this contribution is smaller given the uncertainty we have in the angular alignment (∼5 millidegrees).

Having shown that the NA can generate spectral lineshapes resembling those characterizing coherently coupled systems, we turn our attention to the following complementary question: Can the NA obscure spectral features of bona fide coherently coupled systems? To answer this question, we inspect T and PL spectra of our perovskite−cavity system for shorter cavity lengths than considered in Figures 2 and 3. Figure 5a−c shows measurements in a parameter range where the q = 7 cavity mode crosses the exciton energy. The energies of the bare cavity mode and exciton are shown as dashed black lines in all panels in Figure 5.

Let us first consider the results for the smallest NA_e shown in Figure 5c. Notice how, as the cavity length decreases, the resonance peak bends away from the empty cavity mode and does not cross the exciton energy (2.397 eV). This anticrossing behavior is characteristic of strong coupling. A simple and intuitive way to estimate the coupling regime (weak vs strong) of our system is by fitting the measured resonances with the eigenvalues of a 2 × 2 Hamiltonian describing our exciton-photon coupled system. The diagonal terms of the Hamiltonian contain the exciton and cavity photon energies. We know the bare exciton energy from A measurements in Figure 1c and the bare cavity photon energy from the relation $f = qc/2L$. The off-diagonal term of the Hamiltonian, that is, the coupling constant, is the only fit parameter in our model. By fitting the low-energy eigenvalue of the Hamiltonian to the resonance observed in the Figure 5c measurements, we estimate a Rabi splitting of 150 meV. This value is well

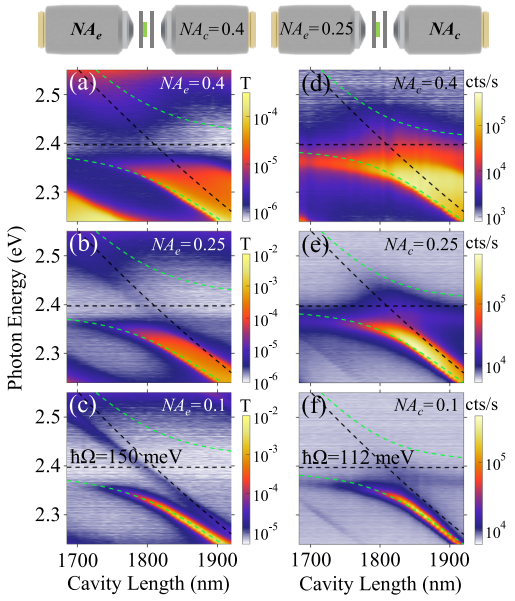

Figure 5. (a−c) Transmittance and (d−f) photoluminescence spectra of the $CsPbBr_3$-cavity system as a function of the cavity length, for a shorter cavity than in Figures 2 and 3. The horizontal dashed black lines indicate the exciton energy, and the tilted dashed black lines indicate the energy of the q = 7 longitudinal cavity mode. The green dashed lines in all panels are the eigenvalues of a 2 × 2 Hamiltonian representing the exciton−photon coupled system. The coupling constant is the only fit parameter, and the result is shown in (c) and (f) for transmittance and photoluminescence measurements, respectively. The coupling was not changed for measurements with different NA.

above the sum of the exciton and cavity photon line widths, which are 66 and 0.5 meV, respectively. Therefore, our exciton−photon system is in the strong coupling regime and the observed resonances correspond to exciton−polaritons. This is not a surprising result. Indeed, strong exciton−photon coupling was recently shown in similar Fabry-Pérot cavities filled with the same perovskite semiconductor. .[30,31] The interesting new observation, enabled by our tunable cavity system, is that the polariton band is so broadened for NA_e = 0.4 that its central energy appears to coincide with the bare cavity mode. Measuring spectra with a single moderately large NA_e only, as done in many works, can lead to the erroneous conclusion that there is no strong coupling. The same holds for the PL measurements shown in Figure 5d−f. These results clearly demonstrate how a moderately large NA can obscure the spectral signature of a bona fide strongly coupled system.

The measurements in Figure 5 display features that require clarification. First, the Rabi splitting observed in PL (112 meV) is smaller than the one observed in T (150 meV). This is consistent with previous calculations[26] and many experimental observations of polariton systems.[27] Second, the upper polariton is not visible in Figure 5 because of above-bandgap absorption. This can be understood in light of the absorbance measurements in Figure 1c. There one can see that absorbance is much greater at energies above the exciton energy, where the upper polariton may be expected but the bandgap absorption sets in. Indeed, previous works reporting exciton−polaritons in optical cavities filled with the same perovskite semiconductor also did not observe the upper polariton.[33]

The energy splitting between upper and lower polaritons at zero detuning (i.e., the Rabi splitting) is the usual indicator of

https://doi.org/10.1021/acsphotonics.1c00128
ACS Photonics 2021, 8, 1271−1276

strong coupling. Since the upper polariton is absent in our data, the accuracy of the coupling constant we determined by fitting to the lower polariton only could be doubtful. We would now like to dissipate this doubt by calculating transmittance spectra as a function of the cavity length for two systems at normal incidence. The calculations are done using the transfer matrix method, and details are provided in Supporting Information. System I is a cavity with $CsPbBr_3$, as in our experiments. The complex refractive index of $CsPbBr_3$ was obtained by applying the Beer−Lambert law to our experimental absorbance data in Figure 1 and then using the Kramers−Kronig relations. This leads to refractive index values that are consistent with previous ones obtained via ellipsometry measurements of $CsPbBr_3$ crystals similar to ours.[34] System II is the same cavity, with $CsPbBr_3$ replaced by a hypothetical material with a single Lorentzian oscillator response. The frequency, line width, and amplitude of that oscillator were chosen such that the resultant complex refractive index matches the one of $CsPbBr_3$ at low energies, where the excitonic response dominates over the bandgap absorption. Comparing these two systems is fair because strong coupling is determined by the excitonic frequency, line width, and oscillator strength, and we are keeping these quantities constant. In the Supporting Information we show the frequency-dependent complex refractive indices of both systems.

Figure 6a,b shows calculation results for systems I and II as described above, respectively. Figure 6a reproduces our

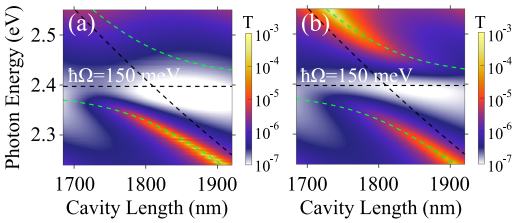

Figure 6. Transmittance, calculated using the transfer matrix method, for a tunable cavity containing a layer representing (a) $CsPbBr_3$, or (b) a material with optical response determined by a single Lorentzian oscillator with the same frequency, line width, and oscillator strength, as the exciton in $CsPbBr_3$. The frequency-dependent complex refractive indices of both systems are shown in the Supporting Information. Green and black dashed lines are exactly the same as in Figure 5. The Rabi splitting obtained empirically from the upper-lower polariton splitting in (b) is equal to the one deduced from fitting to the lower polariton in Figure 5c.

experimental observations from Figure 5c, where the upper polariton is absent. The upper polariton reveals itself when the above-bandgap absorption is removed and the excitonic response is retained, as Figure 6b shows. More importantly, notice that the lower polariton dispersion is practically the same in the two systems. For reference, we superimposed (not fitted) the Hamiltonian eigenvalues from Figure 5c on Figure 6a,b. Notice the excellent agreement between the eigenvalues and the lower polariton energies in both transfer matrix calculations. Moreover, the coupling constant obtained from the fitting (150 meV) exactly reproduces the Rabi splitting which can be empirically (i.e., without any fitting) determined in Figure 6b. This demonstrates the accuracy of the coupling constant deduced from the fitting.

In conclusion, we have shown that a moderately large numerical aperture can artificially generate and obscure spectral features of coupled light−matter systems. In particular, we have seen Fano-like resonances and apparent Rabi splittings entirely due to the incoherent sum of transmitted intensities at different angles collected by the *NA*. Moreover, we have seen how the spectral signature of a bona fide strongly coupled system, the Rabi splitting, can be obscured in measurements with a large *NA*. While these results were obtained using a tunable Fabry-Pérot cavity, we believe that the spectral artifacts we report can also be found in other dispersive nanophotonic systems of contemporary interest, such as plasmonic gratings and metasurfaces. In general, Fano-like lineshapes can be artificially generated whenever the resonance frequency of an optical mode is not constant across the angular range of the measurement. Meanwhile, spectral features resembling Rabi splittings can emerge whenever the frequency separation between two (orthogonal) modes is smaller than the apparent line widths, which are artificially broadenend by the numerical aperture. These spectral artifacts can be avoided by measuring with the smallest possible *NA*, such that the resonance frequency is constant over the limited angular range of the *NA*. Alternatively, angle-resolved measurements can also avoid pitfalls. We recognize that these recommendations may be difficult to implement when measuring the transmission of small samples, as is often the case in nanophotonics research. In that case, a full energy-angle-resolved theoretical study reproducing the measured lineshapes with good accuracy seems to be the only way to assess the true nature of Fano-like lineshapes and Rabi-like splittings. In any case, the mere experimental observation of spectral lineshapes resembling Fano resonances or Rabi splittings cannot by itself be taken as solid evidence of coherent optical phenomena.

■ ASSOCIATED CONTENT

Supporting Information

The Supporting Information is available free of charge at https://pubs.acs.org/doi/10.1021/acsphotonics.1c00128.

Details on transfer matrix calculations (PDF)

■ AUTHOR INFORMATION

Corresponding Author

Said R. K. Rodriguez − *Center for Nanophotonics, AMOLF, 1098, XG, Amsterdam, The Netherlands;* orcid.org/0000-0001-8124-7643; Email: s.rodriguez@amolf.nl

Authors

Zhoumuyan Geng − *Center for Nanophotonics, AMOLF, 1098, XG, Amsterdam, The Netherlands*

Johanna Theenhaus − *Center for Nanophotonics, AMOLF, 1098, XG, Amsterdam, The Netherlands*

Biplab K. Patra − *Center for Nanophotonics, AMOLF, 1098, XG, Amsterdam, The Netherlands;* orcid.org/0000-0003-0592-4344

Jian-Yao Zheng − *Center for Nanophotonics, AMOLF, 1098, XG, Amsterdam, The Netherlands*

Joris Busink − *Center for Nanophotonics, AMOLF, 1098, XG, Amsterdam, The Netherlands*

Erik C. Garnett − *Center for Nanophotonics, AMOLF, 1098, XG, Amsterdam, The Netherlands;* orcid.org/0000-0002-9158-8326

Complete contact information is available at:

https://doi.org/10.1021/acsphotonics.1c00128
ACS Photonics 2021, 8, 1271−1276

https://pubs.acs.org/10.1021/acsphotonics.1c00128

Notes

The authors declare no competing financial interest.

■ ACKNOWLEDGMENTS

This work is part of the research programme of The Netherlands Organisation for Scientific Research (NWO). We thank Femius Koenderink for stimulating discussions. S.R.K.R. acknowledges an ERC Starting Grant with Project Number 852694.

■ REFERENCES

(1) Miroshnichenko, A. E.; Flach, S.; Kivshar, Y. S. Fano resonances in nanoscale structures. *Rev. Mod. Phys.* **2010**, *82*, 2257−2298.
(2) Luk'yanchuk, B.; Zheludev, N. I.; Maier, S. A.; Halas, N. J.; Nordlander, P.; Giessen, H.; Chong, C. T. The Fano resonance in plasmonic nanostructures and metamaterials. *Nat. Mater.* **2010**, *9*, 707−715.
(3) Törma, P.; Barnes, W. L. Strong coupling between surface plasmon polaritons and emitters: A review. *Rep. Prog. Phys.* **2015**, *78*, 013901.
(4) Limonov, M. F.; Rybin, M. V.; Poddubny, A. N.; Kivshar, Y. S. Fano resonances in photonics. *Nat. Photonics* **2017**, *11*, 543−554.
(5) Garrido Alzar, C.; Martinez, M.; Nussenzveig, P. Classical analog of electromagnetically induced transparency. *Am. J. Phys.* **2002**, *70*, 37−41.
(6) Joe, Y. S.; Satanin, A. M.; Kim, C. S. Classical analogy of Fano resonances. *Phys. Scr.* **2006**, *74*, 259−266.
(7) Rodriguez, S. R.-K. Classical and quantum distinctions between weak and strong coupling. *Eur. J. Phys.* **2016**, *37*, 025802.
(8) Hao, F.; Sonnefraud, Y.; Dorpe, P. V.; Maier, S. A.; Halas, N. J.; Nordlander, P. Symmetry Breaking in Plasmonic Nanocavities: Subradiant LSPR Sensing and a Tunable Fano Resonance. *Nano Lett.* **2008**, *8*, 3983−3988.
(9) Offermans, P.; Schaafsma, M. C.; Rodriguez, S. R. K.; Zhang, Y.; Crego-Calama, M.; Brongersma, S. H.; Gómez Rivas, J. Universal Scaling of the Figure of Merit of Plasmonic Sensors. *ACS Nano* **2011**, *5*, 5151−5157.
(10) Yu, Y.; Heuck, M.; Hu, H.; Xue, W.; Peucheret, C.; Chen, Y.; Oxenløwe, L. K.; Yvind, K.; Mørk, J. Fano resonance control in a photonic crystal structure and its application to ultrafast switching. *Appl. Phys. Lett.* **2014**, *105*, 061117.
(11) Sheikholeslami, S. N.; García-Etxarri, A.; Dionne, J. A. Controlling the Interplay of Electric and Magnetic Modes via Fano-like Plasmon Resonances. *Nano Lett.* **2011**, *11*, 3927−3934.
(12) Yan, C.; Yang, K.-Y.; Martin, O. J. Fano-resonance-assisted metasurface for color routing. *Light: Sci. Appl.* **2017**, *6*, No. e17017.
(13) Doeleman, H. M.; Dieleman, C. D.; Mennes, C.; Ehrler, B.; Koenderink, A. F. Observation of Cooperative Purcell Enhancements in Antenna−Cavity Hybrids. *ACS Nano* **2020**, *14*, 12027−12036.
(14) Yu, Y.; Xue, W.; Semenova, E.; Yvind, K.; Mork, J. Demonstration of a self-pulsing photonic crystal Fano laser. *Nat. Photonics* **2017**, *11*, 81−84.
(15) Yang, K. Y.; Skarda, J.; Cotrufo, M.; Dutt, A.; Ahn, G. H.; Sawaby, M.; Vercruysse, D.; Arbabian, A.; Fan, S.; Alù, A.; Vučković, J. Inverse-designed non-reciprocal pulse router for chip-based LiDAR. *Nat. Photonics* **2020**, *14*, 369−374.
(16) Hutchison, J. A.; Schwartz, T.; Genet, C.; Devaux, E.; Ebbesen, T. W. Modifying Chemical Landscapes by Coupling to Vacuum Fields. *Angew. Chem., Int. Ed.* **2012**, *51*, 1592−1596.
(17) Feist, J.; Galego, J.; Garcia-Vidal, F. J. Polaritonic Chemistry with Organic Molecules. *ACS Photonics* **2018**, *5*, 205−216.
(18) Rodriguez, S. R. K.; Casteels, W.; Storme, F.; Carlon Zambon, N.; Sagnes, I.; Le Gratiet, L.; Galopin, E.; Lemaître, A.; Amo, A.; Ciuti, C.; Bloch, J. Probing a Dissipative Phase Transition via Dynamical Optical Hysteresis. *Phys. Rev. Lett.* **2017**, *118*, 247402.
(19) Laussy, F. P.; Kavokin, A. V.; Shelykh, I. A. Exciton-Polariton Mediated Superconductivity. *Phys. Rev. Lett.* **2010**, *104*, 106402.
(20) Orgiu, E.; George, J.; Hutchison, J.; Devaux, E.; Dayen, J.; Doudin, B.; Stellacci, F.; Genet, C.; Schachenmayer, J.; Genes, C.; Pupillo, G.; Samorí, P.; Ebbesen, T. Conductivity in organic semiconductors hybridized with the vacuum field. *Nat. Mater.* **2015**, *14*, 1123−1129.
(21) Coles, D. M.; Yang, Y.; Wang, Y.; Grant, R. T.; Taylor, R. A.; Saikin, S. K.; Aspuru-Guzik, A.; Lidzey, D. G.; Tang, J. K.-H.; Smith, J. M. Strong coupling between chlorosomes of photosynthetic bacteria and a confined optical cavity mode. *Nat. Commun.* **2014**, *5*, 1−9.
(22) Su, R.; Diederichs, C.; Wang, J.; Liew, T. C. H.; Zhao, J.; Liu, S.; Xu, W.; Chen, Z.; Xiong, Q. Room-Temperature Polariton Lasing in All-Inorganic Perovskite Nanoplatelets. *Nano Lett.* **2017**, *17*, 3982−3988.
(23) Ramezani, M.; Halpin, A.; Fernandez-Dominguez, A. I.; Feist, J.; Rodriguez, S. R.-K.; Garcia-Vidal, F. J.; Gomez Rivas, J. Plasmon-exciton-polariton lasing. *Optica* **2017**, *4*, 31−37.
(24) Delteil, A.; Fink, T.; Schade, A.; Höfling, S.; Schneider, C.; İmamoğlu, A. Towards polariton blockade of confined exciton−polaritons. *Nat. Mater.* **2019**, *18*, 219−222.
(25) Muñoz-Matutano, G.; Wood, A.; Johnsson, M.; Vidal, X.; Baragiola, B. Q.; Reinhard, A.; Lemaître, A.; Bloch, J.; Amo, A.; Nogues, G.; Besga, B.; Richard, M.; Volz, T. Emergence of quantum correlations from interacting fibre-cavity polaritons. *Nat. Mater.* **2019**, *18*, 213−218.
(26) Savona, V.; Andreani, L. C.; Schwendimann, P.; Quattropani, A. Quantum well excitons in semiconductor microcavities: Unified treatment of weak and strong coupling regimes. *Solid State Commun.* **1995**, *93*, 733−739.
(27) Schwartz, T.; Hutchison, J. A.; Genet, C.; Ebbesen, T. W. Reversible Switching of Ultrastrong Light-Molecule Coupling. *Phys. Rev. Lett.* **2011**, *106*, 196405.
(28) Melnikau, D.; Esteban, R.; Savateeva, D.; Sánchez-Iglesias, A.; Grzelczak, M.; Schmidt, M. K.; Liz-Marzán, L. M.; Aizpurua, J.; Rakovich, Y. P. Rabi Splitting in Photoluminescence Spectra of Hybrid Systems of Gold Nanorods and J-Aggregates. *J. Phys. Chem. Lett.* **2016**, *7*, 354−362.
(29) Rodriguez, S. R. K.; Murai, S.; Verschuuren, M. A.; Rivas, J. G. Light-Emitting Waveguide-Plasmon Polaritons. *Phys. Rev. Lett.* **2012**, *109*, 166803.
(30) Du, W.; Zhang, S.; Shi, J.; Chen, J.; Wu, Z.; Mi, Y.; Liu, Z.; Li, Y.; Sui, X.; Wang, R.; Qiu, X.; Wu, T.; Xiao, Y.; Zhang, Q.; Liu, X. Strong Exciton−Photon Coupling and Lasing Behavior in All-Inorganic CsPbBr3Micro/Nanowire Fabry-Pérot Cavity. *ACS Photonics* **2018**, *5*, 2051−2059.
(31) Su, R.; Ghosh, S.; Wang, J.; Liu, S.; Diederichs, C.; Liew, T. C.; Xiong, Q. Observation of exciton polariton condensation in a perovskite lattice at room temperature. *Nat. Phys.* **2020**, *16*, 301−306.
(32) Zhang, Q.; Su, R.; Liu, X.; Xing, J.; Sum, T. C.; Xiong, Q. High-Quality Whispering-Gallery-Mode Lasing from Cesium Lead Halide Perovskite Nanoplatelets. *Adv. Funct. Mater.* **2016**, *26*, 6238−6245.
(33) Su, R.; Wang, J.; Zhao, J.; Xing, J.; Zhao, W.; Diederichs, C.; Liew, T. C.; Xiong, Q. Room temperature long-range coherent exciton polariton condensate flow in lead halide perovskites. *Sci. Adv.* **2018**, *4*, No. eaau0244.
(34) Chen, X.; Wang, Y.; Song, J.; Li, X.; Xu, J.; Zeng, H.; Sun, H. Temperature Dependent Reflectance and Ellipsometry Studies on a CsPbBr3 Single Crystal. *J. Phys. Chem. C* **2019**, *123*, 10564−10570.